ANALYSIS AND DESIGN OF RAPID PROTOTYPED MECHANISMS USING HYBRID FLEXURAL PIVOTS

BY

JORGE EDUARDO CORREA P.

THESIS

Submitted in partial fulfillment of the requirements
for the degree of Master of Science in Mechanical Engineering
in the Graduate College of the
University of Illinois at Urbana-Champaign, 2015

Urbana, Illinois

Adviser:

Professor Placid Mathew Ferreira

ABSTRACT

The ability of fabricating flexure based mechanism is of great importance in modern technology fields such as nanotechnology and precision engineering. For an instance, a great number of nanopositioning systems are made out of flexures. Examples of these systems are those used in scanning probe microscopy and many other types of metrology tools. Not having friction is a requirement to achieve nanometer scale motion and thus flexural systems are preferred as they lack of sliding surfaces. Moreover, flexure hinges are able to produce accurate and repeatable motion when properly designed. Conventionally, flexure-type systems are manufactured from high performance metals such as stainless and alloyed steel or aluminum alloys for high material performance and durability. Functional requirements such as high bandwidth, accuracy performance and geometric complexity require them to be manufactured as monolithic structures using conventional precision machining and electro discharge machining (EDM). However, such an approach is expensive and not practical for mass production. They can only be used for custom and high-value added applications. Conventional and emerging additive manufacturing technologies such as Direct Metal Laser Sintering (DMLS) offer an opportunity to fabricate cost effective flexure-based mechanisms with complicated spatial structures. However, the reported limitations of this approach are: dimensional accuracy, low quality surface finish, anisotropic properties, thermal instability, low holding force capabilities and severely reduced durability of the flexural elements as most rapid prototyping materials are unsuitable in fatigue loading conditions. This thesis work envisions an approach to manufacture hybrid mechanisms that uses *i)* economic methods like casting and molding (for high volume production) or 3-D printing (for custom, one-off systems) for manufacturing the mechanism structures/skeletons and *ii)* inserts of simple geometry with specialized materials (e.g. spring steel, etc.) to get the right material properties where need it.

The objective of this research is to develop and exemplify a methodology that integrates a host material (rapid prototyping) with a flexure material and combines them to create a much more easy to produce mechanism. For this purpose, we focus on the design of the interfaces between the two materials and, particularly, the penetration depth of the insert into the host. Using Finite Element simplified model and tracking mechanical variables such as stress, pressure and elastic energy we arrived to the functions relating the optimum penetration depth (insertion

distance where the elastic work done by the host material is minimum relative to that one done by the flexure) with the thickness of the flexure and the elastic properties of the two materials. For example, in the case of an aluminum host and steel inserts; the optimum penetration distance is six times the thickness of the insert whereas in the case of an ABS structure and steel inserts, the optimum penetration desistance is ten times greater than the insert thickness. Further results include the study of extra compliance introduced to the system in design scenarios considering materials and manufacturing consideration for the fabrication, alignment and assembly of the mechanism. Finally, we demonstrate a piezoelectric-actuated four-bar mechanism, and an XYZ force sensor for suture training as general applications of these devices to the precision motion field and the medical industry. The methodology implemented in this work poses a simple and affordable way to fabricate, assemble and customize low-cost devices for precision motion application and it applies to both, systems fabricated by polymer and metal rapid prototyping technologies.

To Father, Mother and Brother

ACKNOWLEDGEMENTS

This project would not have been possible without the support of many people. I would like to begin by thanking my adviser, Professor Placid M. Ferreira for giving me the opportunity to work under his supervision in his group, as well for his unconditional support and advice both in the technical aspects of this work and the personal and developmental arena.

I would like to thank my close friends and colleges Bruno Azaredo, Nicholas Toombs, Shama Farabi, Numair Ahmed and Bonjin Koo and Kyle Jacobs. This work would not have been possible if it was not for their help, constant support and because of the wonderful working environment they provided. Furthermore, I would like to thank to the undergrad students in the MechSE department who help me in this project, particularly, Nikhil Kapoor whose hard work and help in the lab where of great importance in the construction of some of the designs presented in this thesis work.

Thanks to my close friends Bruno Azaredo, Ricardo Toro, Ana Arango, Maria Piñeros, Nicholas Toombs and Shama Farabi, for always offering company, support and love. Thanks to the University of Illinois and the MechSE department staff with providing me with the human resources and economical means to complete this project.

Finally, thank to my parents and brother for their continuous support, love and guidance from Colombia while I studied at the University of Illinois.

TABLE OF CONTENTS

LIST OF FIGURES

CHAPTER 1: INTRODUCTION

Flexure based mechanisms are of great importance in modern technology application fields such as micro and nanopositioning, trajectory scanning and several probe/tool based metrology. A flexure is a compliant element that provides relative motion between adjacent rigid members through controlled flexing. They are particularly relevant to precision engineering because of their ability to amplify or attenuate a mechanical input in a repeatable and controlled way [1], [2]. Conventionally, flexure-type systems are manufactured from high performance metals such as stainless and alloyed steel or aluminum alloys for high material performance and durability [3] [4] [5] [6] [7]. Functional requirements such as high bandwidth, accuracy performance and geometric complexity require them to be manufactured as monolithic structures using conventional precision machining and electro discharge machining (EDM) (See fig. 1). However, such an approach is expensive and not practical for mass production. They can only be used for custom and high-value added applications. More recently, rapid prototyping technology (RP) has been proposed and implemented in the fabrication of cost-effective flexure-based mechanisms with complicated spatial structures ([8], [9], [10], [11] and [12]). Some of the advantages of using rapid prototyping in the fabrication of flexure-based mechanisms are: quick product testing, ease-of-design iteration, elimination of design errors, workspace validation, evaluation of singular configurations and link interference determination. However, the reported limitations are: dimensional accuracy, low quality surface finishing, anisotropic prosperities, thermal instability, holding force capabilities. Severely reduced durability of the flexural elements as most rapid prototyped materials are unsuitable in fatigue loading is a particularly debilitating drawback.

We envision an approach that uses economic methods like casting and molding (for high volume production) and 3-D printing (for custom, one-off systems) for manufacturing the complex geometry of the structural parts of the systems, flexural elements of simple geometry with specialized materials (e.g. spring steel, etc.), and well-design interfaces between the two. This paper presents a design methodology for prototyped mechanism with hybrid-flexural pivots and proposes a process for their fabrication. In this study, finite element simulations are used to understand the mechanical behavior of these elements and to produce optimal design for

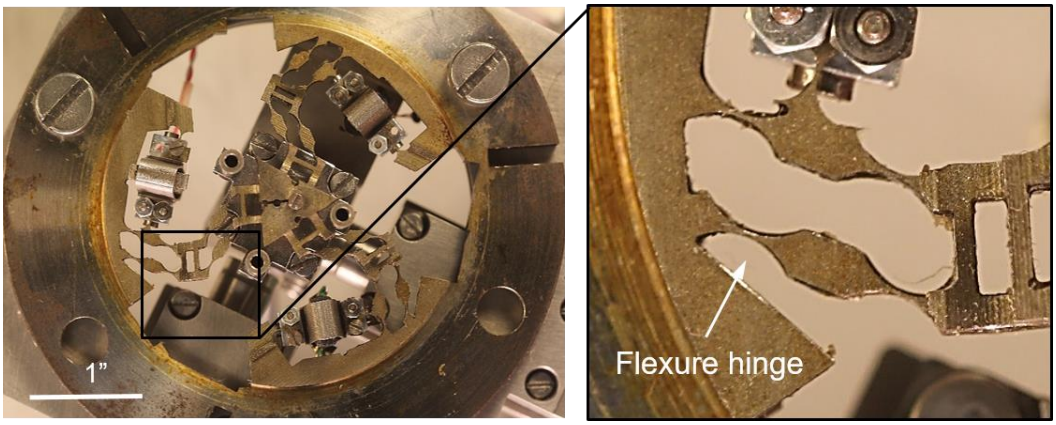

Figure 1. An XYZ parallel kinematics mechanism manufactured using wire EDM.

the aforementioned interfaces between components. In the proposed fabrication process, the links in device structure are prototyped as a single monolithic piece, held together by sacrificial structures or tabs. This is followed by the insertion of metallic leafs, press-fitted into place to complete what we call the hybrid flexural pivots. The hybrid pivots, in the designs described here, allow for relative rotations between the different links of the mechanism. Finally, the holding or sacrificial tabs are snapped off and the devices are ready for operation. This methodology combines the ability and effectiveness of Rapid Prototyping in economically creating complicated spatial structures with the superior mechanical properties of metallic inserts, necessary for the flexural components. This provides numerous advantages for the design of precision motion systems such as: (a) rapid and affordable customization, (b) rapid fabrication, (c) time and cost saving, and (d) designs that are suitable for light-weight applications.

An important aspect of this design and fabrication strategy is the interface between the rigid links (which might be made of many different materials including polymers, additively deposited metals, and cast metals) and the flexural elements. The joints that result are what we refer to as hybrid flexural pivots.

1.1. Motivation

To exemplify the necessity of a practical, low-cost approach to manufacture flexure based mechanisms, we go back to the parallel kinematics machine for XYZ nanopositioning shown in figure 1. This mechanism is a typical example of conventional manufacture of flexure based mechanism. The physical realization of this machine required four different wire EDM setups due to the three-dimensional complexity of this structure (required to transform the in-plane motion of the actuators into translational motion of the end-effector in three independent axis). It becomes clear that this type of approach although beneficial for the production of one off systems, is very expensive and impractical for mass-production implementation. Another example of the necessity of a new approach to the manufacture of flexure based mechanism can be found in our laboratory. Here, we are constantly seeking for innovative flexure-based machine designs and motion schemes with potential applications to the precision engineering area. However, the costs and times associated to the manufacturing of this devices represents one of the principal challenges of this type of research. Because of this, it is desirable to develop a manufacturing platform that enables fast, iterative design that can be incorporated with conventional mass manufacturing technologies and, more importantly, that offers realistic functionality.

Emerging adding manufacturing technologies and conventional polymer extrusion and casting are readily available and have the potential to been used as a fast iteration platform for the design of flexure based mechanism with complex geometry. However, the overall material

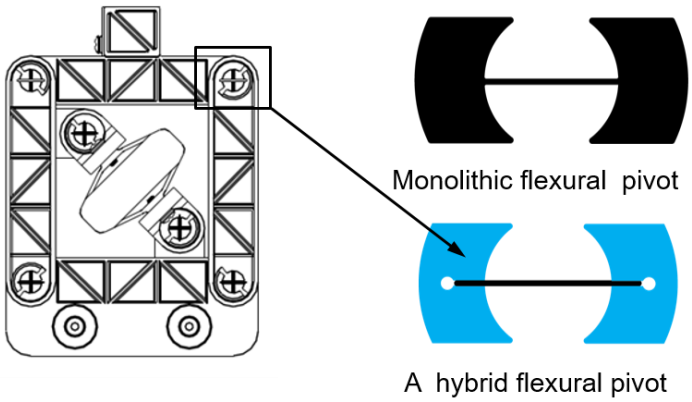

Figure 2. A Four-bar hybrid mechanism with hybrid flexural pivots

properties of plastics and resulting properties from this processes are not suited for flexural elements. [1]To address this challenges, we proposed the concept of hybrid mechanisms whereby plastic structures are molded or rapid prototyped containing the link arrangement of the mechanism and higher-properties inserts are used to allow relation motion between the links and to get the right material properties where needed. Such approach would represent a cost effective strategy to the fast iterative design of flexure based mechanisms and their adaptation

1.2. Objectives of this research

This research focuses efforts in developing a design methodology that integrated a host material, produced by rapid prototyping casting or molding, with a flexure material and combine them to create a much more easy to produce mechanism of comparable mechanical behavior. The hybrid mechanisms in this context are composed by hybrid flexural pivots. We define a hybrid flexural pivot to be a compliant joint designed to produce limited relative rotation between two adjacent rigid parts. The rigid parts are attached to each other by means of metallic inserts acting as leaf springs and allowing the relative rotation between them through flexing. Figure 2 shows an example of a four-bar hybrid mechanism with hybrid flexural pivots. Here, the inserts are easy to manufacture using technologies such as wire EDM, water jet, laser cutting or metal sheet forming. Each of the traditional processes works well and the objective of this methodology is to make them work together to form a hybrid flexure-based mechanism. Ideally, like flexing in the hybrid joints takes place about the midpoint of the flexural leaves attaching the tubes [2]. The hybrid flexural pivots are designed to have constant stiffness, minimum parasitic motion and behave elastically throughout their range of motion.

Finally, this thesis exemplifies the design methodology with potential applications to the precision engineering field and the medical instrumentation area

[1] The resulting microstructure of this processes and the layered-based aspect of rapid prototyping technologies produces inferior overall material properties.

CHAPTER 2: METHODOLOGY

The design criterion in this methodology focuses on tracking relevant mechanical quantities, such as pressure, stress and strain energy, at the insert/host interface. For this purpose, FEM (finite element method) structural analysis is used to quantify these interactions. With this information, we are able to arrive to optimal dimension of these interfaces that result in beneficial distributions of this mechanical quantities in the two elements.

Even though the design of the overall flexure dimensions is not in the scope of this work, (there already exist a variety of techniques available to the design of flexural pivots and flexure hinges given the stiffness, range of angular displacement and form factor of the application) a brief description of the pin-joint model [13] is used as a first design approach to estimate the flexural pivots stiffness.

2.1. The pin-joint model

In the pin-joint model by Jensen and Howell [13], one can conceptually think of the joint as having a rigid pin located at the center of the flexural pivot, shown in Fig. 3. Then, we have the joint stiffness given by:

$$K = \frac{K_\theta EI}{2l} \tag{1}$$

Where K is the rotational stiffness of the pivot, E is the Young's modulus of the material and I is the moment of inertia of the flexible section and l is the length of the flexible segments. K_θ is regarded as the stiffness coefficient and it is a function of the dimensionless parameter n defined as the ratio of the effective pivot length r and the in-plane pivot width h (see Fig. 3)**.** To use the pin-joint model, the value of the stiffness coefficient K_θ needs to be determined first. K_θ is determined by minimizing the deflection error of the cross-axis flexural pivot through a motion of 1.1 radians for different values of the dimensionless parameter, n. Afterwards, a polynomial curve fit is used, yielding the function. The authors report the following polynomial equation for the value of K_θ;

$$K_\theta = 5.300185 - 1.6866n + 0.885356n^2 - 0.2094n^3 + 0.018385n^4 \tag{2}$$

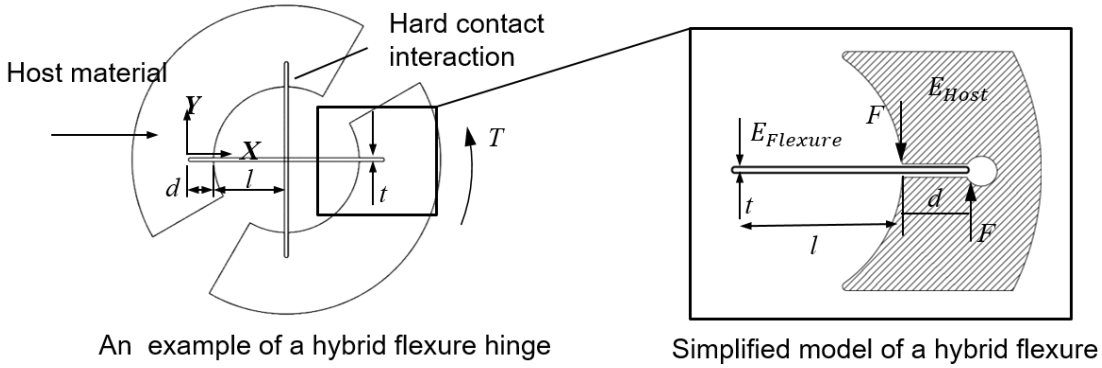

Figure 3. Hybrid flexure simplified model

With $0.5 \leq n \leq 4.0$. To exemplify the methodology, the flexural pivots of this work have dimensions t = 0.254 mm, l = 5 mm and width w = 5mm. Then, the parameter n equals 1. The material used is steel with Young's modulus E = 200 GPa and a proportional limit of 480 MPa. A metal flexural pivot with these materials and dimensions has a rotational stiffness coefficient K_θ = 4.30792 and rotational stiffness K = 0.5767 N m/rad. Here, we used the pin-joint model as initial criteria to estimate the dimensions of the hybrid cross-axis flexural pivots such as length, thickness and width of the springs as well as to evaluate its load-deflection characteristics.

It should be noted that actual stiffness properties of the hybrid flexures will defer from the values obtained from the pin-joint model as the latter neglects the energy dissipations due to the contact interactions. Nonetheless, the pin-joint model still a valid tool that can be used as a starting point to estimate the initial parameters of the hybrid-flexures.

2.2 Mechanics of hybrid flexural pivots

To study the mechanics of hybrid flexural pivots and, particularly, the mechanics at the hybrid interfaces, we use the simplified plain-elasticity model in figure 3. This abstraction is valid under the assumptions of symmetry in the joints, the host material been widely distributed around the interfaces, i.e. $R>>d + l$, and, finally, no apparent variation of geometry in the out-of-plain direction. These assumptions guarantee that high magnitudes in the stresses and strain-energy fields are confined near the interfaces between the flexures and the host material and, therefore, the following study can focus on the detailed design of this interfaces.

The geometrical parameters of the simplified model are the thickness of the insert t, the effective length of the flexure l, the reacting force F at the interface due to the action of the

actuation torque *T*, the width of the flexure *w*, and the penetration distance of the insert into the host material *d*. E_{host} and $E_{flexure}$ are the elastic modules of the host and the flexure materials respectively.

The idea here is use this simplified model to track mechanical variables such as stress, pressure and energy distribution between the components of the flexures and contact pairs to find geometries of the host/flexure interfaces that minimize the amount of elastic work done by the host material with respect to the flexures. For this purpose we define the optimum penetration depth d_{opt} as the insertion distance of the flexure into the host material distance when the elastic work done by the host material is minimized with respect to the flexure. To make the result of our analysis scalable, we define the following normalizing quantities.

2.2.1 Average opening pressure at the interface

This average opening pressure results from evenly distributing the reaction force *F*, due to the external torque *T*, along the contact area of the interface. This quantity is mathematically defined as

$$\sigma_{\infty} = \frac{F}{2A} = \frac{T}{2d^2 w} \tag{3}$$

2.2.2 Strain energy in an equivalent monolithic flexure

This quantity represents the elastic energy that would be stored in a monolithic flexural pivot of same dimension and subjected to the same loading torque *T*. The mathematical expression for the expression for the strain energy in an equivalent monolithic flexure can be obtain with the help of the stiffness relations in Eq. (1) and is computed as

$$U_{\infty} = \frac{K\theta^2}{2} = \frac{K_{\theta} E_m I_m \theta^2}{4l} \tag{4}$$

Now that we have identified a set of mechanical quantities and normalizing factors to study the performance of different interfaces, we are ready to use parametric FEM (finite element method) structural analysis to obtain numerical values of the stress and energy field in our hybrid flexure.

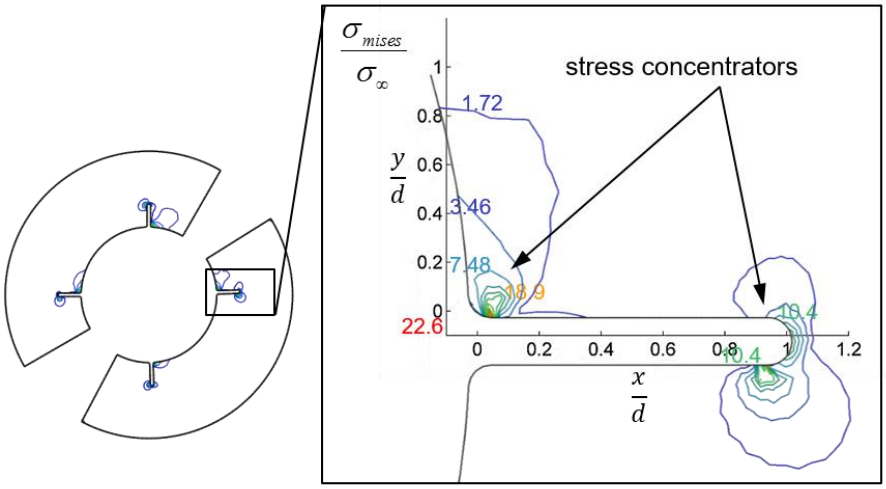

Figure 4. Von Mises stress field isocontours in the host material

2.3 Finite element model

Our FEA model is a two-dimensional computer implementation of the simplified model shown in figure 3. In this model, the hybrid flexural pivot is under the action of a counter-clock wise torque applied to one of its rigid ends and held fixed by the other one. The structural simulations were implemented in Abacus CAE as a plain elastic problem with constant thickness *w* and hard contact interactions at the interfaces formed by the polymer and the metallic elements.

Typically, with this types of model and materials, the interfaces have high stress concentration points. This concentration causes lots of undesired deformation resulting in parasitic motions or the introduction of extra compliance in the flexure. Fig. 4 shows the Von Mises stress field isocontours in the host material normalized by the average pressure at the interface. In this graph, the *x* and *y* coordinates are also normalized by the penetration distance *d.* The Von Mises stress field reveals that the stress concentrators can be as high as twenty times the average stress at the interface and, further, that there exist two main mechanisms of stress concentration, namely, the localized contact pressure between the flexures and the host structures at opposite sides of the interface and the stress distribution at the tip of the notch resulting from the opening of the groove. High concentrations of stresses at the interface (in the side of the host material) results in significant amounts of undesired extra-compliance of the pivot.

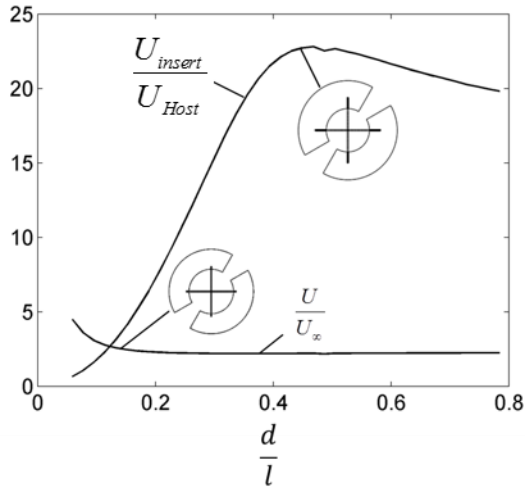

Figure 5 Strain energy distribution as a function of the ration d/l.

Although the previous FEA simulations demonstrated the challenges associated when designing around this types of interactions, a more detailed study is required to find the geometry that optimizes the structural behavior of this hybrid couple. For this purpose, the following section used parametric FEA to understand the influence of the effective flexural length *l*, the thickness of the flexures *t*, and the selection of materials in the proper selection of the optimum penetration depth $d_{opt.}$

2.4 Parametric FEA simulation

To motivate the concept of optimum penetration depth, let us device a computational experiment in which the strain energy in the host material and the flexures is plotted for increasing penetration depths. The parameters for the simulation are t = 0.254 mm, l =5mm and $E_{host}/E_{flexure}$ = 69 [2]. To present the results of this experiments, we define U_{host} to be the total strain energy stored in the host material. In the same way, $U_{flexure}$ is the strain energy stored in the flexures and, finally, U is the total strain energy in the hybrid flexure. These quantities can be obtained by integration of the strain-energy density fields in the individual domains of the FEA model. Further, we recall U_∞, from our previous discussion (See Eq. (4)), to be the total

[2] This selection of parameters correspond to the case of an ABS host material and a steel flexure

strain energy in an equivalent monolithic flexure. Figure 5 shows the result of this experiments in two different plots. The first plot shows the ratio of the strain energy in the insert to the strain energy in the host, for increasing penetrations. The second plot shows the ratio of total strain energy stored in the hybrid flexure to the strain energy store in an equivalent monolithic flexure. While the former describes the energy distribution in the different components of the joint, the latter describes how much elastic energy is stored in the hybrid flexure compared to one made of a single material. This relates to the extra-compliance created by the introduction of a host material and the contact interaction. It is observed from this study that for penetration distances grater that 20% of the effective length of the flexure, the total elastic energy stored in the hybrid pivot is constant and further increasing the penetration distance would only change its distribution between the components. At this point, it is easy to identify that the optimum penetration depth occurs when the penetration distance is 50% of the effective length of the flexure and that for this interface geometry selection the flexure component work around twenty times harder than the host. At higher penetration depths (d / l >> 0.5), the compliance of the notch structure becomes relevant resulting in a higher value of strain energy stored in the host material.

This preliminary example demonstrated the existence of an optimum penetration distance and elucidated its importance as design criteria to produce hybrid interfaces with minimum the undesired interactions. However, the influence of effective flexural length l, the thickness of the flexures t, and the selection of materials in the calculation of the optimum penetration depth d_{opt} still

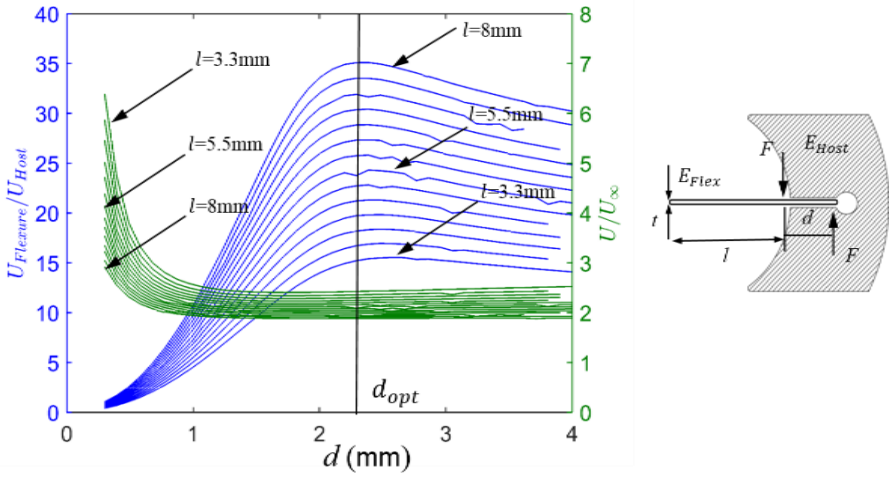

Figure 6. Optimum penetration distance vs. flexure length

unexplored. To address this questions, in the following subsection, we will add complexity to our analysis by allowing this parameters (l, t, $E_{host}/E_{flexure}$) to vary in addition to the variation in the penetration depth.

2.4.1 Optimum penetration distance as a function of the flexure effective length

In this parametric study, we start by allowing the penetration distance to vary, from 0.5 mm to 4mm, at a flexure length of 3.3 mm and repeat this process for increasing lengths up to 8 mm. The model parameters t = 0.254 mm and $E_{host}/E_{flexure}$ = 69 are held constant throughout the simulations. Figure 6 shows the results of the parametric analysis. We use the left vertical axis to plot the ratio of the strain energy in the insert to the strain energy in the host, for different flexure length and increasing penetrations. In the same manner, we use the right vertical axis to plot the ratio of total strain energy stored in the hybrid flexure to the strain energy store in an equivalent monolithic flexure. Much like in our previous experiment (section 2.4), we identify the existence of an optimal penetration depth at a distance d = 2.2 mm, for the selected model parameters, regardless the length of the flexures.

From the graph, it can be observed that high flexural lengths result in more beneficial distributions of elastic energy in the hybrid joints and, more importantly, they result in overall elastic properties that resemble more closely those ones of a monolithically fabricated flexural pivot. The intuition for this can be found in the fact that the lateral stiffness in the flexure decreases with the cube of its length and, therefore, as the length of these insert increases, their

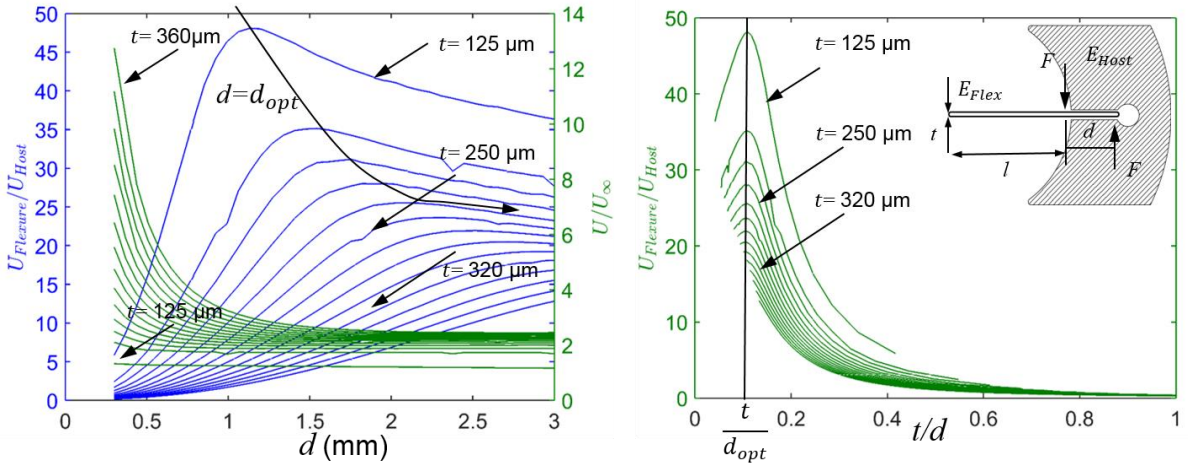

Figure 7.Optimun penetration distance vs. flexure thickness

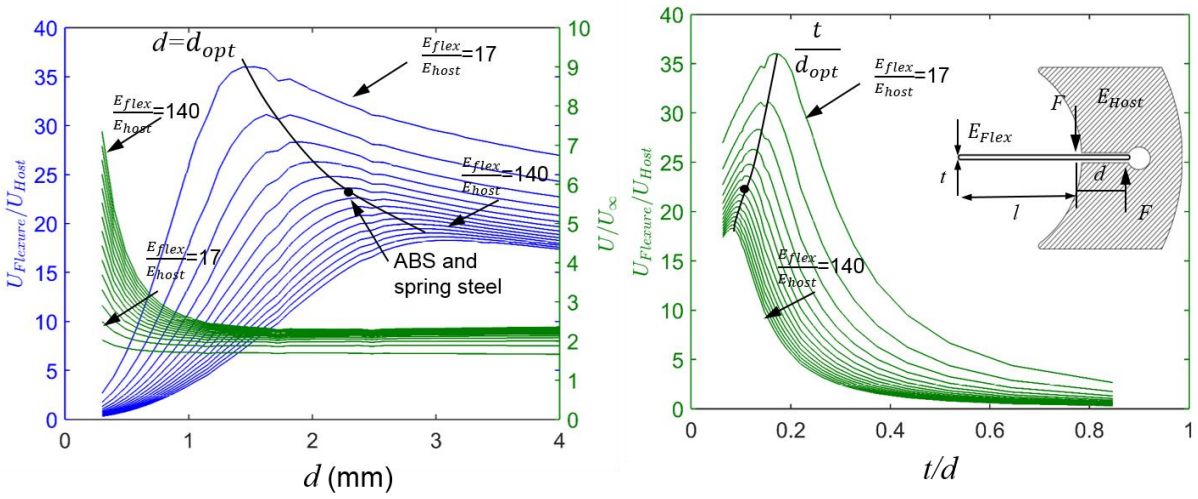

Figure 8.Optimun penetration distance vs. young modulus ratio

compliance becomes dominant in the system which is an ideal situation.

2.4.2 Optimum penetration distance as a function of the flexure thickness

In this section, we want to understand the influence of the thickness of the flexure in the computation of optimum penetration depth. To capture this effect, we allow the penetration distance to change for an initial value of 0.5 mm to a final value of 4 mm, at a flexure thickness of 125 µm and repeat this process for increasing lengths up to 360 µm. In this set of simulation, the length of the flexure and the ration of elastic modules of the host to the flexure materials are kept constant at values of 5mm and 69 respectively.

Figure 5 (left) uses the left vertical axis to plot the ratio of the strain energy in the insert to the strain energy in the host and the right vertical axis to plot the ratio of total strain energy stored in the hybrid flexure to the strain energy store in an equivalent monolithic flexure. From the results of this simulations we observe that the optimal penetration depth is a function of the thickness of the flexure, particularly, the penetration distance should increase for thicker flexures. It can also be concluded that thinner flexures correspond to more beneficial distributions and flexures that resemble more closely their monolithically fabricated counterparts. This can be explain form the fact that thinner flexures have increased compliance; as the compliance of this elements becomes dominant in the system, more energy is store in elastic flexing than deformation of the host material.

At this point, we have identified the optimal penetration depth on the flexures thickness. To get a better idea on which type of dependence, figure 7 (right) shows the energy distribution in the joint as a function of the dimensionless quantity *t/d.* From this graph, it becomes clear that the optimum penetration distance varies linearly with the thickness of the flexure and that it must be around ten times the thickness of the flexure for the selection of materials in this simulation.

2.4.3 Optimum penetration distance as a function of the material properties

Now that we know that the optimum penetration depth is a function of the thickness of the material, we move forward to study its dependence on the selection of materials in the hybrid flexures. In this final set of simulations, we allow the penetration distance to vary form 0.5 mm to 4 mm at a starting ratio of elastic modulus of the materials of 17 (this corresponds to the case of a host made of aluminum and flexures made of steel) and repeat this process for increasing young module rations up to 150.

Figure 8 (left) shows that the optimal penetration depth is also a function of the Young modulus ration of the materials in the hybrid flexure. Namely, less penetration depth is required as the host material becomes stronger. The hybrid flexures act more like monolithically fabricated flexures and have a more beneficial distribution of strain energy for stronger host materials. Figure 8 (right) presents the elastic energy distribution in the hybrid joint as a function of the dimensionless quantity *t/d* for different selections of materials. From this graph, it can be observed that the optimum penetration depth is a continuous function of the selection

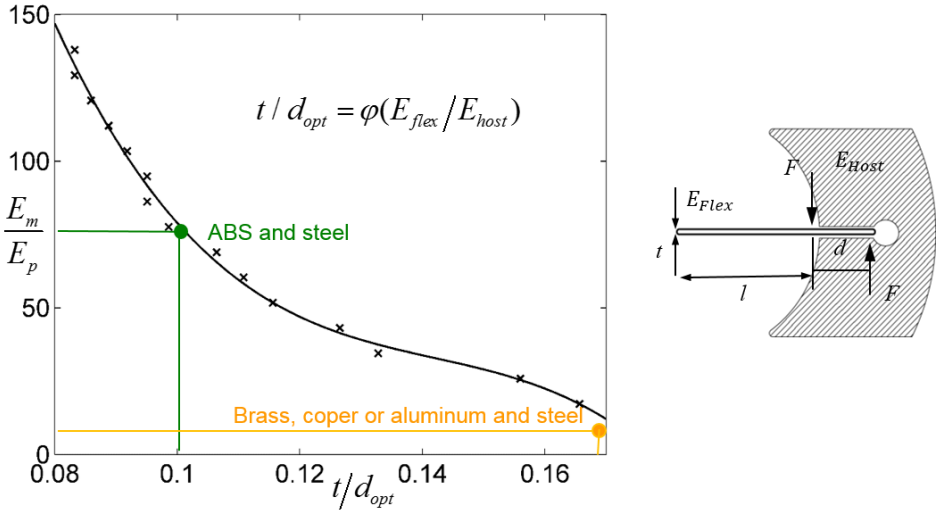

Figure 9. Non-dimensional relation to find the optimum penetration distance d_{opt}

of materials in the flexure and that as the properties of the host materials approach the properties of the flexure, the constraint of the penetration distance been ten time the thickness of the flexure gets relaxed.

2.4.4 Result of the parametric finite element model

From a designing perspective, the thickness of the flexure, length and the selection of materials are independent of whether the flexure is manufactured using a conventional or a hybrid fashion. These parameters are determined by application requirements such as range of motion, bandwidth, stiffness and shape factor and they can be obtained from standard relations available in the literature [1, 2] . In this methodology work, the design problem is stated as: given the basic flexure geometry and its materials, find the optimal penetration distance that minimizes the unwanted mechanical interactions. To address this problem, we construct the non-dimensional relation $t/d_{opt} = \varphi(E_{flex}/E_{host})$ by combining the previously identified data on the behavior of optimum penetration depth as a function of the thickness of the flexures and the selection of materials. Figure 9 shows the relation between the ratio of materials elastic module with respect to the nondimensional number t/d_{opt}. For example, in the case of an aluminum host and steel inserts the optimum penetration distance is six times the thickness of the insert whereas in the case of an ABS structure and steel inserts, the optimum penetration desistance is ten times greater than the insert thickness.

So far, our discussion has focus on the problem of finding the optimum penetration distance for a hybrid flexural pivot where the flexure is clamped at its ends by the horst material. The following section explores the idea of evolution of contact pressure at the interface followed by its delamination. Additional considerations to minimize undesired interactions in the interface are arrived by studding the contact stresses for increasing loading conditions.

2.4.5 Interface fit analysis

In a typical loading situation (see Fig. 3), a torque *T* is applied to one of the ends of the pivot while the other one is held fixed. The action of this torque is transmitted to bending of the flexure by means of the force couple *F*. In an ideal case, these forces are evenly, or at least gradually distributed along the area of contact. However, in the absence of contact pressure, the reacting forces are localized at opposite sides of the interface giving rise to high stress concentrations that, in turn, change the load-deflection behavior of the flexure.

An interference fit can been applied to keep the interface in contact (for a designed range of motion), and attenuate the stress concentrations. To generalize the results in our computational model, we define the preload stress as the normalizing stress required to open the clamp, in the host material, a distance δ. The preload stress can be computed, from elasticity theory, as

$$\sigma_{\infty 1} = \frac{\sqrt{2} E_{host} \delta}{4d(1-\nu^2)} \tag{5}$$

Where d is the penetration distance and ν is the Poisson ratio of the host material. In this analysis, we also use the normalizing flexing stress (previously defines as the average pressure at the interface in section 2.2) defined as

$$\sigma_{\infty 2} = \frac{T}{2d^2 w} \tag{6}$$

To capture the interference fit effect in our computational model, we brake the boundary conditions of the problem in two steps and use superposition principle. This assumption is valid for small deformations of the flexure. Figure 10 (left) shows the basic steps in the simulation. First, the interference δ is defined (step 1) as a mismatch between the flexure thickness and the initial opening of the interface. This interference causes a preload stress distribution in both materials (step 2). Finally, the boundary condition corresponding to the external torque is imposed to the system resulting in a flexing stress distribution. The total intensity of this two fields can be estimated by the total average stress defined as

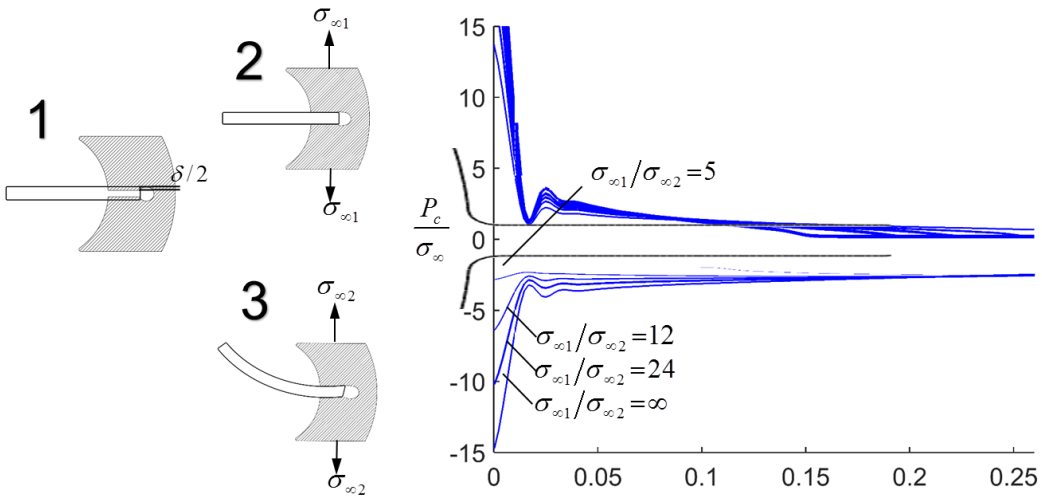

Figure 10. Evolution of the normalized pressure interface

$$\sigma_{\infty} = \sigma_{\infty 1} + \sigma_{\infty 2} \quad \textbf{(7)}$$

Figure 2 (right) presents the evolution of the normalized pressure at interface (normalized the by total average stress) for different rations of preload stress to flexing stress. Initially, a preloading condition exists and the flexing stresses are zero. This corresponds to the case $\sigma_{\infty 1} / \sigma_{\infty 2} = \infty$. At this point, the pressure distributions on the top and button surfaces of the interface are symmetrical. The pressure profile at one on the sides of the interface attenuates while the other intensifies as the external torque is allowed to gradually increase. Our simulations show that delamination might take place when the intensity of the flexing stress reaches a value of around five times the intensity of the preload one.

The previous analysis provides a systematic way to calculate the required amount of interference for a required rotation of the flexure. However, this study is incomplete in the sense that it disregards the elastic limits of the host material and, therefore, it cannot be used as failure criteria.

2.4.6 Fracture mechanics-based failure criteria for flexural pivots

In this section, we propose a fracture mechanics approach to formulate failure criteria for our hybrid flexural pivots. Such approach is valid for the case where the localized contact stresses are well attenuated by the selection of a proper penetration depth and interference fit (sections 2.4.1 to 2.4.5) and, thus, the mechanism of failure becomes the stress distribution at the tip of the notch that results from the opening the clamp. To illustrate this concept, we use our

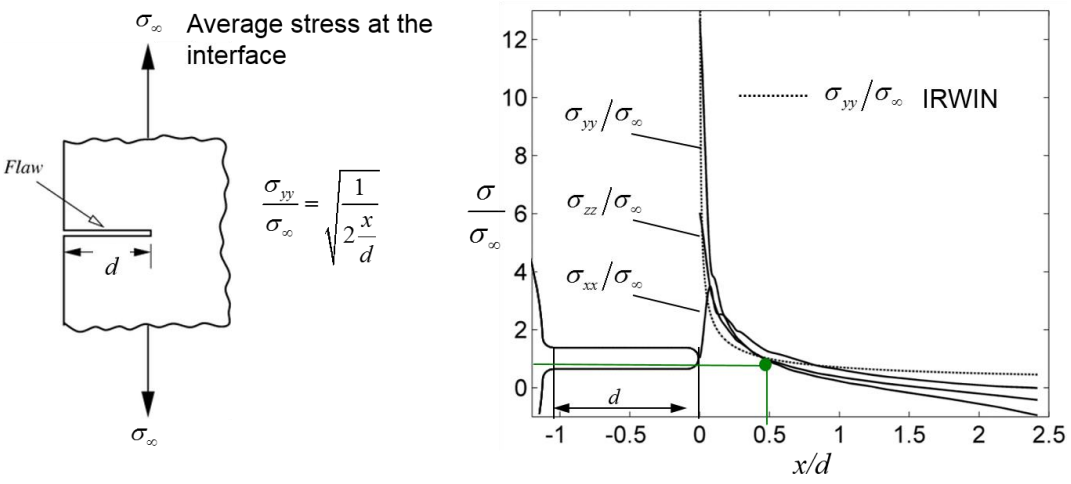

Figure 11. Normalized normal stress near the tip of the opening

computational model to extract the different normal stresses and normalized them by the average pressure at the interface. Figure 11 shows the result of these simulations. To validate the assumption of having stress distributions similar to that encounter in fracture, we recall the definition of stress intensity factor K_I in polar coordinates

$$\sigma_{yy} = \frac{K_I}{\sqrt{2\pi x}} f_{yy}(\theta) \tag{8}$$

Where σ_{yy} is the normal stress in the vertical direction and f_{yy} is a dimensionless quantity that varies with the geometry. Further, f_{yy} is equal to one along the horizontal axis. Also, from the Irwin definition of stress intensity factor, we have

$$K_I = \sigma_\infty \sqrt{\pi d} \tag{9}$$

Where σ_∞ is the amplitude of the stresses applied to open the crack or in our case, the average opening pressure at the interface. The theoretical normalized value of σ_{yy} is obtained by taking the ration between equations (8) and (9) as

$$\frac{\sigma_{yy}}{\sigma_\infty} = \sqrt{\frac{1}{2\frac{x}{d}}} \tag{10}$$

Figure 11 also shows the Irwin theoretical values for the normalized σ_{yy} stress as a dotted line. It can be observed, from the graph, that this distribution is fairly close to the one obtained numerically using finite element simulations. This verifies our previous assumption of having a fracture stress distribution near to the tip of the opening. This result provides the opportunity of using the Irwin definition of stress intensity factor in Eq. (9) as a failure criteria for our hybrid flexures. Here, the underlying idea is to experimentally identify values limiting values of K_I for different set of materials and dimensions of the interface.

CHAPTER 3: MANUFACTURING AND TESTING OF THE HYBRID FLEXURES

This section is an introduction to the manufacturing aspects and challenges encounter in the fabrication of hybrid flexures. To exemplify this challenges, we choose stereo lithography apparatus (SLA) rapid prototyping technology because of its easiness of implementation and its availability in our facilities. However, we would like to remind the reader that the methodology and fabrication aspects in this work can be applied to more scalable manufacturing technologies with higher process capabilities such as polymer molding or casting.

3.1 Rapid prototyping of the joints

Because of the anisotropic properties of the printed material, resulting from the layer-based additive manufacturing process, the CAD models of the joint parts must be properly oriented in order to achieve the desired strength near the contact interfaces (See Fig. 12). Deposition of layers oriented parallel to the flexures axis of rotation, result in increased strength of the host material structure in the directions of the forces transmitted by the inserts. The flexural pivots were adapted for fabrication using the ViperTM SLA system. Due to the process capabilities of layer thickness of 25 µm (in high resolution mode), it is difficult to achieve smooth-vertical surfaces with repeatable interference distances (between the insert and the host parts). Nevertheless, this should not discourage the use of rapid prototyping technologies in this type of application as the design principles of this thesis work can be mapped to the growing Direct Metal Laser Sintering (DMLS) technology, which has the potential of producing stronger and denser parts that would allow for tighter interference clearances corresponding to better control of contact pressures at the insert-host interfaces.

To produce functional hybrid joints, a trial error experiment was device in which previously

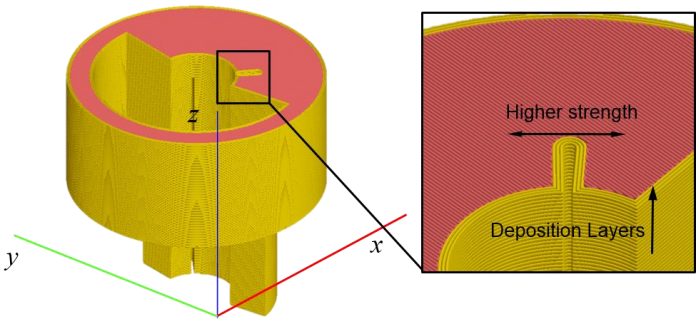

Figure 12 Example of a sliced part properly oriented

cut metallic leaf springs were inserted into different printed structures. In these experiments, we used the SLA materials water clear Ultra 10122 and ProtGenTM O-XT 18420 (See figure 13). Although, the parts made of water clear Ultra10122 exhibited better dimensional accuracy, the ProtGen is a more suitable choice for this application due to its higher toughness. The trial and error process resulted in interference clearances of 50 µm.

3.2 Assembly and testing of the joints

The assembly of the joint is achieved by manual press fitting, with vertical forces around 2.5 Kg. The dimensional accuracy and surface finish of the mating surfaces are important fabrication considerations that pose challenges to the SLA process. Different alternatives for the assemblage of the flexures include the use of screws, epoxy adhesives and interlocking geometries between the flexures and the slots.

To test the load-deflection of the design components, we designed a simple cantilever beam with a flexural pivot acting as torsional spring and attached different weights to it. A picture of the setup is shown in Fig.14. The critical dimensions of the flexure are those ones specified in the example of section 2 as per the pin-joint model. The length of the cantilever arm is 50 mm. To obtain the load-displacement behavior, different weights with incremental values ranging between 1g and 20g were sequentially attached to the end-tip of the cantilever. The corresponding values of deflection were extracted by capturing images at the corresponding equilibrium configuration with a pixel resolution of 10 µm. The measured data was post-processing using image software to correct for the registration issues in the setup. Fig 14 also presents the load deflection characteristics of the system. It can be seen form the graph that the flexure stiffness starts with an initial value of 0.1375 N.m/rad for smaller angles of deflection and as the twist angle increases, the stiffness of the flexure increases to a value of

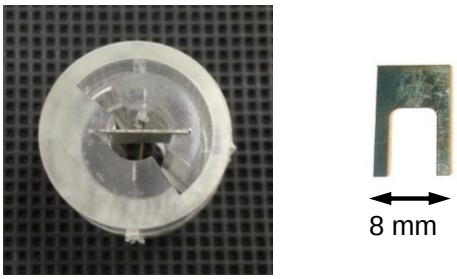

Figure 13. Assembly of a hybrid flexural pivot using SLA water clear material and a wire EDM spring-steel insert

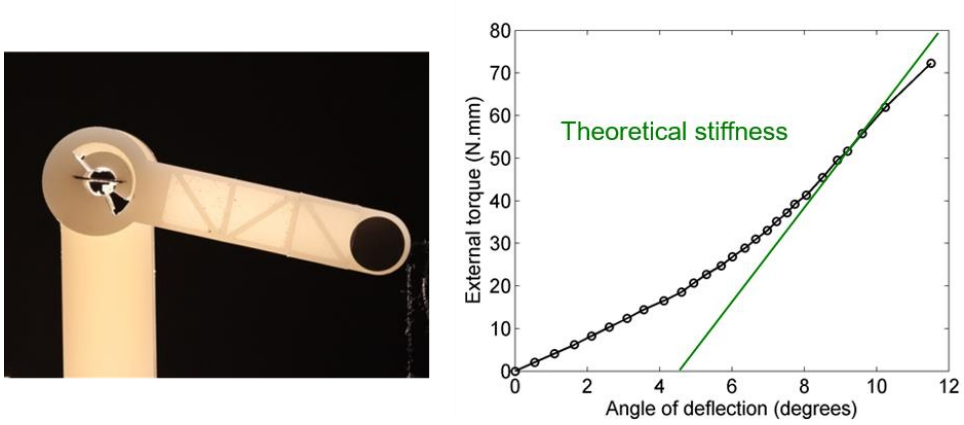

Figure 14. A prototyped cantilever beam with a hybrid flexural pivot and its load-deflection behavior

0.5913Nm/rad. The change in stiffness suggests the existence of backlash between the insert and the host structure due to low tolerance control in the SLA process. The play in the joint prevents the inserts to fully contact the host surfaces during the early stages of motion.

CHAPTER 4: CASE STUDIES

This section of the thesis offers examples of two different devices in the areas of health training and nanopositioning designed using hybrid flexures. Particularly, we demonstrate a 4-bar compliant mechanism for single degree-of-freedom positioning systems and a three axis load sensor for force measurements in possible medical applications We decided to test our design methodology in this fields because they represent direct applications of some of the research topics in our laboratory and also because they are very successful at demonstrating the versatility, rapidness and performance of this design approach.

4.1 Piezoelectric actuated 4-bar mechanism

A parallelogram four-bar mechanism embedded, with hybrid flexural pivot joints was prototyped, assembled and tested (Fig. 15). A piezoelectric actuator was chosen because of its size, bandwidth and actuation force capabilities. For the sake of compactness, the actuator is assembled inside the parallelogram with the line of actuation forming an angle of 45 degrees with the crank of the mechanism. To reduce the bending torque experienced by the actuator, this one is mounted between two flexural pivots attached to the crank and to the base of the device. The mechanism consists of six flexural pivots each of them having two metallic leaf springs. The solid model and the prototype version of the mechanism with the actuator connected are shown in Fig.15. The chosen actuator is a CEDRAT APA40, with free stroke 52 µm, blocking force of 194N and a maximum driving voltage of 150V. The chosen dimensions for the crank and follower were 45 mm. The end effector has a total displacement of 28 µm corresponding to a rotational range of the hinges of 0.04 degrees. For this ranges of angular displacement, the loss of

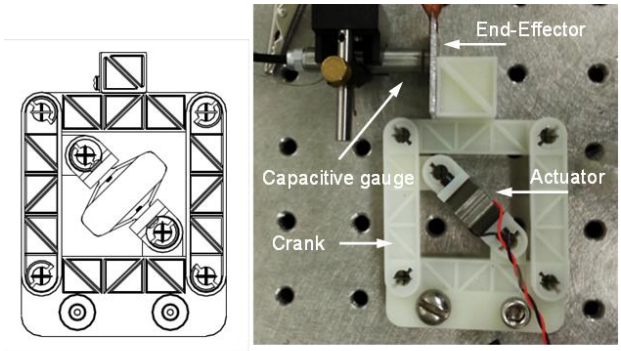

Figure 15 CAD model and (b) prototype of piezoelectric actuated mechanism

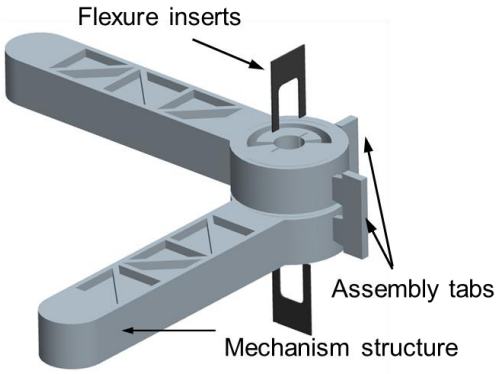

Figure 16 Assembly of bars using tabs

parasitic motion in the vertical direction are 1.12 nanometer and the changes in angular stiffness of the hybrid joints are negligible. Capacitive sensors (Probe 2805 and Gauging Module 4810 ADE Technologies) are used to directly capture the motion of the end effector. The target for the capacitive sensor is a polished aluminum plate glued to the end-effector of the four bar mechanism.

One of the chalenges of manufacturing hybrid flexure-based systems is registration and aligment. It it difficult to manually assamble the individual components of the mechanisms with the inserts without yiending low gemetrical tolerances. To address this issue, the mechanism structure was prototyped as a whole and held together by plastic tabs (without the inserts parts would naturally fall apart). Figure 16 shows two adjoint prototyped linked held together by assembly tabs. After the insertion of the flexures, the tabs are snapped from the structure and the mechanism is released.

4.1.1 Static response

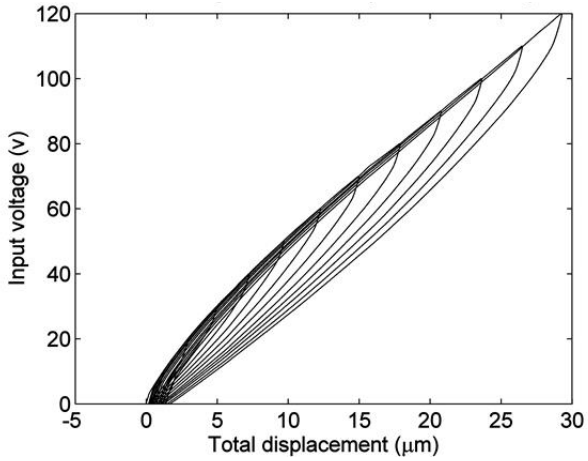

Figure 17 Voltage-displacement plots for piezoelectric actuated mechanism

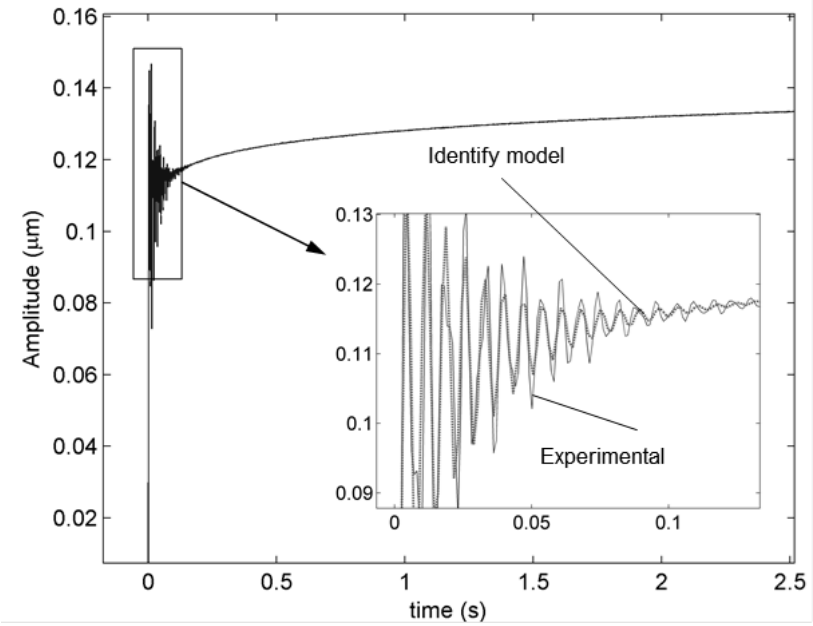

Figure 18 Step response of piezoelectric actuated 4-bar mechanism

To study the static behavior of the device, the input voltage to the actuator was sequentially ramped up at increasing values, from 0 volts to 120 volts in increments of 10 V, and plotted against the end-effector motion observed by the capacitive sensor. The signal was generated at a low frequency (0.015 Hz) to rule out the dynamic effects. The results of this experiment are reported in Fig. 17. For the small angular displacement of the hybrid pivots, the hysteresis and loss of motion in the system are due to the piezoelectric actuator rather than the mechanical response of the structure. This hypothesis was validated by carrying out the same experiment with the piezoelectric actuator disengaged from the mechanism.

4.1.2 Dynamic response

To capture the dynamics of the system, a step input of 1 volt was introduced to the actuator while the position of the end-effector was recorded by the capacitive sensor. Fig. 17 shows the step response of the system. The identified damped natural frequency for the system is 140 Hz. To gain further understanding of the dynamics of the system, the Bode plot of the open-loop response was generated using a dynamic signal analyzer. Figure 18 shows the amplitude and phase diagrams when the input frequency is sweep between the values of 5 Hz and 1000 Hz near to the equilibrium point, at a constant amplitude of 4 V. The experimental data shows that the damped resonant frequency of the system is consistent with the 140 Hz of damped natural frequency obtained from the step response. The frequency response also indicates that the open-

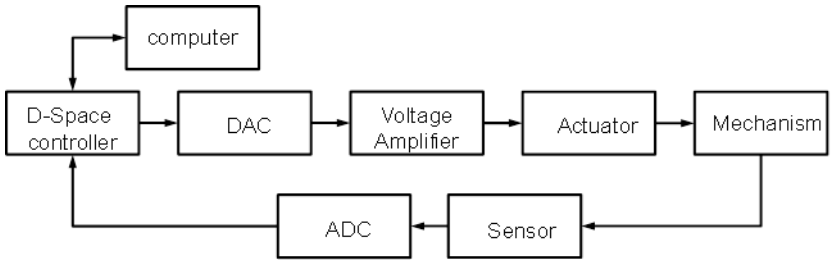

Figure 19. Close loop control scheme

loop bandwidth of the system is 50 Hz as the gain and the phase lag of the system remain constant below this value. A transfer function of the system was identified using both the experimental step input and frequency response as:

$$G(s) = \frac{-0.06031S^2 + 243.8S + 154.6}{S^2 + 517.6S + 277.2} \tag{11}$$

The zeros in the system account for the hysteretic behavior of the piezoelectric actuator. The experimental and identified step responses of the system are shown in Fig. 18.

4.1.3 Closed-loop tracking performance

Tracking performance and contouring accuracy are central characteristics for micropositioning systems. To test the performance of the prototyped mechanism a PI controller was designed based on the experimental observation of the system. In a trial an error methods in which the proportional action was the main control, the integral action was used to refine the tracking performance. This procedure resulted in. The controls of the device were implemented using a D-space motion controller. Fig 19 shows the close loop scheme for the PI controller. In this scheme, sine waves of different frequencies were generated with the D-space controller and

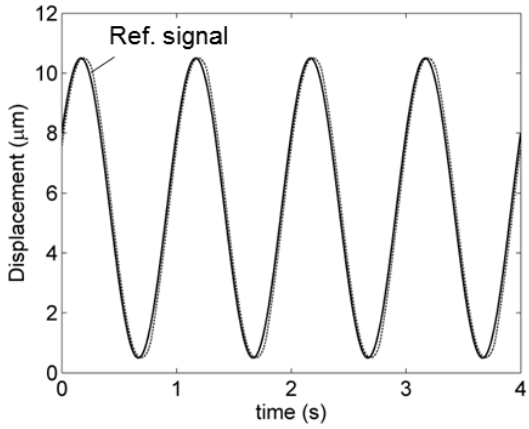

Figure 20 4-bar mechanism tracking performance

Table 1. Sinusoidal tracking results

Max. Speed (um/s)	Max. error (nm)	Average error (nm)
20	32.6	17.8
40	164.1	19.1
80	169.4	38.2
160	176.4	42.7

used as reference signals. The reading form the capacitive sensor was used as feedback and the error between the reference and sensing signals was used as the input for the PI controller. A DAC system together with an amplifier were used to convert the controller signal to the analog voltage ranges of the piezoelectric actuator and to digitalize the reading from the capacitive sensor back to the controller. Tracking tests were conducted by driving the mechanism along a sinusoidal trajectory with amplitude of 5 um an top speeds ranging from 0 to 80 um/s. Fig. 19 shows the time response of the system at a driven speed of 80 μm/s . The results of the sinusoidal tracking test are summarized in table 1. The maximum tracking error at 80 um/s is less than 180 nm and the average contouring error is less than 50 nm.

4.2 Flexure-based XYZ-Force sensor for medical training applications

Knot tying and suturing are fundamental skills that require a level of coordination used by surgeons and may other types of professionals. Traditionally, these technical abilities are gained through practice during and after training. However, assessment of the quality of these tasks has always been subjective and based on observation by experts. This training and evaluation costs medical residents and attending surgeons operating time and the improperly tied knots can cause tissue damage and other expensive complications. Currently, training is completed on a mechanical tie board and the lack of feedback and monitoring make it a less than ideal solution. Virtual reality is now used for training purposes, but there is not much feedback involved, costs are too high, and there are underdeveloped methods of force detection.

This application focuses on the design of a device that can be used as a quantitative way of understanding the forces involved in any process that requires fine manual skills such as surgery and microassembly. The produced device needs to be able to evaluate forces in all directions, be compact and sensitive, and also, be small so that it can be easily embeddable in different environments without perturbing the measurements. The solution we developed is a xyz-force

sensor based on our hybrid-flexure schemes of manufacturing that incorporates a nested stricture to achieve spatial translations. This solution is multi-faceted in that it has strong potential in many applications such as the control of the quality of the motion produced and it provides a mean of evaluating and certifying the level of dexterity of the test taker.

4.2.1 Functional description of the system

The design, fabrication and test of the flexure-based XYZ force sensor is made possible by the introduction of hybrid-flexures that facilitated its manufacturing and design iteration process within a highly compact nested structure. The structure is the result of the integration of an X–stage into a Y-stage that is also embedded into an outer-most Z stage. Each of the stages is composed by a set of leaf-springs arranged into a parallelogram 4-bar mechanism designed so that their connector undergoes pure translation. Initially, each stage moves in a direction that is orthogonal to the others. The sensing mechanism consists of attaching strain gauges to the flexures of the individual stages and relating the forces applied to the moving stage to the electrical signal generated by the deflection of leafs. The device is fabricated based on a low cost approach that uses water-jet technology to manufacture the leaf-springs and 3D printing to produce parts that interface the leaf-spring with the structural elements of the stages.

The sensor operates under a pure translational scheme and relies on the principle that a force acting of the moving plate can be decomposed into a unique combination of motions of the stages. The form-factor of our design was conceived by dividing the shell of a cube into identical l-shape parts and interconnecting them via flexural springs. The end-effector and the

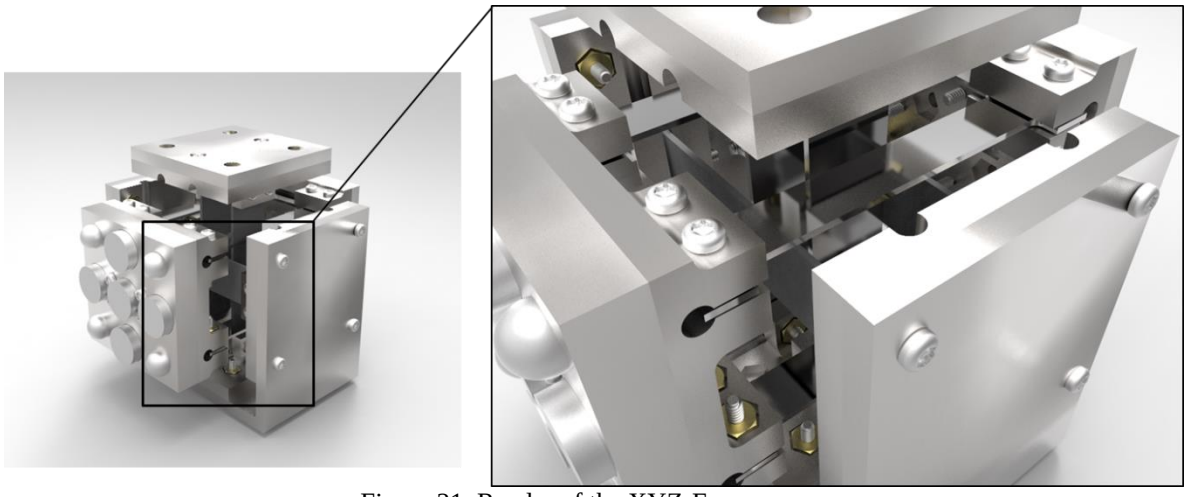

Figure 21. Render of the XYZ-Force sensor

moving plate are the result of further splitting one of the l-parts into two perpendicular plates. The detailed design of the stage is shown in Figs. 22 and 23. Figures 23(a) - 23(c) show the sequential assembly of the stages while Fig. 23(d) show the final design of the sensor. In this scheme, the one degree-of-freedom stages connects the fixed plate to the moving plate in series. Each stage consists on a beam-type translational joint with multiple flexures. The beam-type translational joint constraints the extra degrees-of-freedom by the parallel arrangement of two or more identical beams that form an equivalent four-bar mechanism. The parallel four-bar mechanism allows one pure translational motion on a curvilinear trajectory. In this architecture, the Z-stage is a four-beam flexure-type translational joint while the X, and Y stages are two-beam type translational joints. This consideration facilitates the nesting of the Y and X axes into the Z-axis. Although the flexure arrangement within the stages is different (The Z-axis has four flexures while the reaming axes have two), the flexures of each stage are designed to have the similar combined static-stiffness.

4.2.2 Static Analysis

The XYZ-force sensor was design for force-measurement applications such as stitching or suturing processes, involving force ranges between 10mN and 2000 mN. This design constraints together with the selection of spring steel as the material for the leaf springs, translates to the

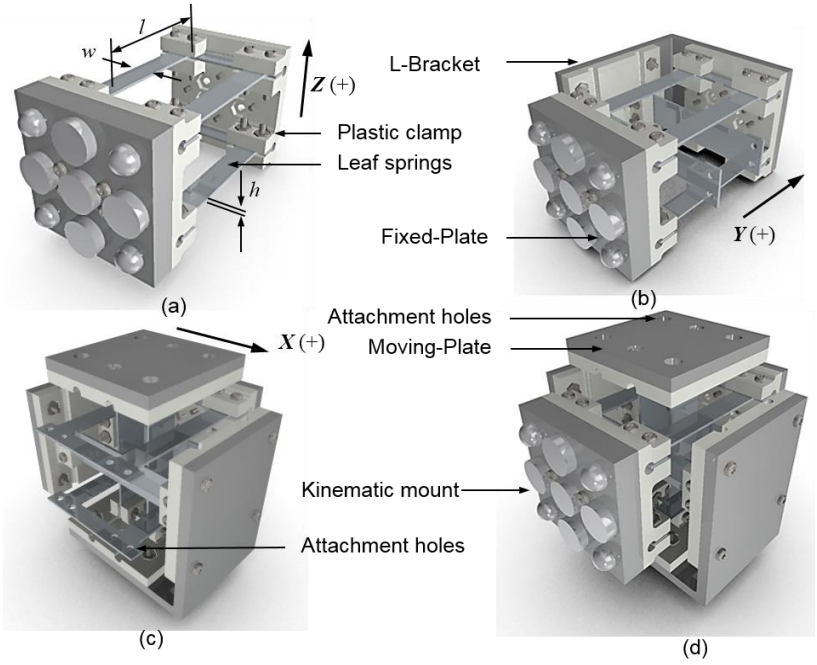

Figure 22. Architecture and assembly sequence of the sensor: (a) the Z stage; (b) the Y stage; (c) the X stage; and (d)

problem of finding the leaf-spring dimensions that produce elastic strain ranges within the ranges of the strain gauges. To find those dimensions, the stiffness of a clamped-clamped beam along the direction of motion K_d and the lateral direction lateral direction K_l can be expressed from elementary beam theory as:

$$K_d = \frac{2Eht^3}{L^3}, K_l = \frac{2Eht}{L} \tag{12}$$

The chosen dimensions for the spring and their stiffness properties are listed in table 2. Even though all stages have similar stiffness in direction of motion, their dynamic characteristics are different because the mass their carried mass is not the same. Particularly, the Z-axis carries both the X and Y-stages and thus, is natural response is slower. The same applies for the Y-stage relative to the X-stage. Table 1, also lists the value of the maximum displacement of each stage δ_{mac}. This value, determines the allowance required between the leafs of the different axes to avoid self-collision during operation. A small separation between the parallel arrangements of springs gives an opportunity for greater allowances but this situation should be avoided to prevent unwanted rotations of the stages.

4.2.3 Fabrication aspects

To reduce the cost of fabrication, the leaf-springs are manufactured in batches by cutting different stacks of spring-steel using a conventional water-jet process. This operation produced sharp contours and well defined clamping holes of 1mm diameter. To assemble the device, the leaf springs are clamped by 3D printed parts that are screwed to stiffening aluminum plates and l-shape brackets. 3D printed was used to avoid the manufacturing cost of complex-geometry parts with the extra consideration of a well design interface between the two components and a larger sized sensor. The l-shape brackets connect the different stages by twisting the direction of motion of the flexures and provide structural stiffness to the sensor .The aluminum plates

Table 2.

	X- axis	**Y-axis**	**Z-axis**
w	5.21 mm	5.21 mm	3.16 mm
h	400 μm	400 μm	381 μm
L	18 mm	18 mm	18 mm
K_d	2.859 N/mm	2.859 N/mm	1.5 N/mm
δ_{max}	0.675mm	0.675 mm	0.7 mm

correspond to the fixed and moving links. A set of threaded holes are located onto the moving plate to mount spatialized measurement tools. The solid model and the prototyped version of the XYZ sensor are shown in Fig.24. All components with the exception of the 3D parts and the leaf-springs where obtained off-the-shelf.

4.2.4 Calibration and instrumentation

The calibration of the XYZ sensor requires a systematic way of loading along the X, Y and Z directions (both in the positive and negative orientations). To avoid a complex setup of pulleys and cables, or the alignment of actuators with the orthogonal directions, a split groove kinematic coupling with 90˚ rotational symmetry was adapted to the fixed plate of the sensor. At the same time, the sensor can be fixed in place to a calibration mount by means of a symmetrical array of magnets placed inside the foot-print of the v-grooves. The magnetic-kinematic mount was designed to have 90˚ rotation symmetry resulting in a repeatable way of orienting the 6 translational DOF of the sensor along the gravity direction. Fig. 23 shows the XYZ sensor with kinematic mount, and its calibration mount.

Linear strain gauges (SGT-2C/350-TY11 from omega) are used to capture the strain near the fixed ends of the springs. In our prototype, one strain-gauge is implemented per stage. However, two strain gauges (one in the top surface and the other one in the bottom) might be used for thermal noise cancelation, output linearity and enhanced resolution. The individual gauges of each axes are arranged in a quarter bridge configuration and the output voltage is amplified with an operational amplifier (OP-Amp). For the acquisition of data, the low cost

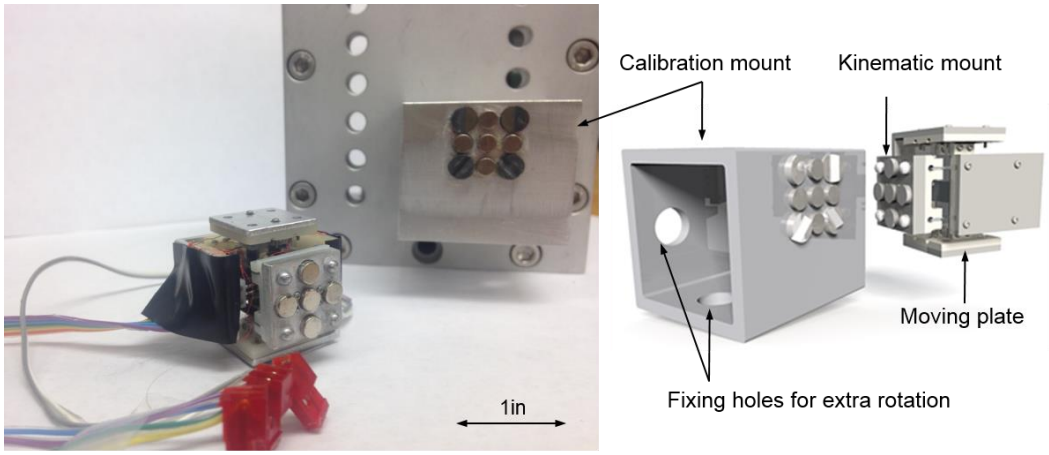

Figure 23 Prototype of XYZ force sensor (a) and its CAD model (b).

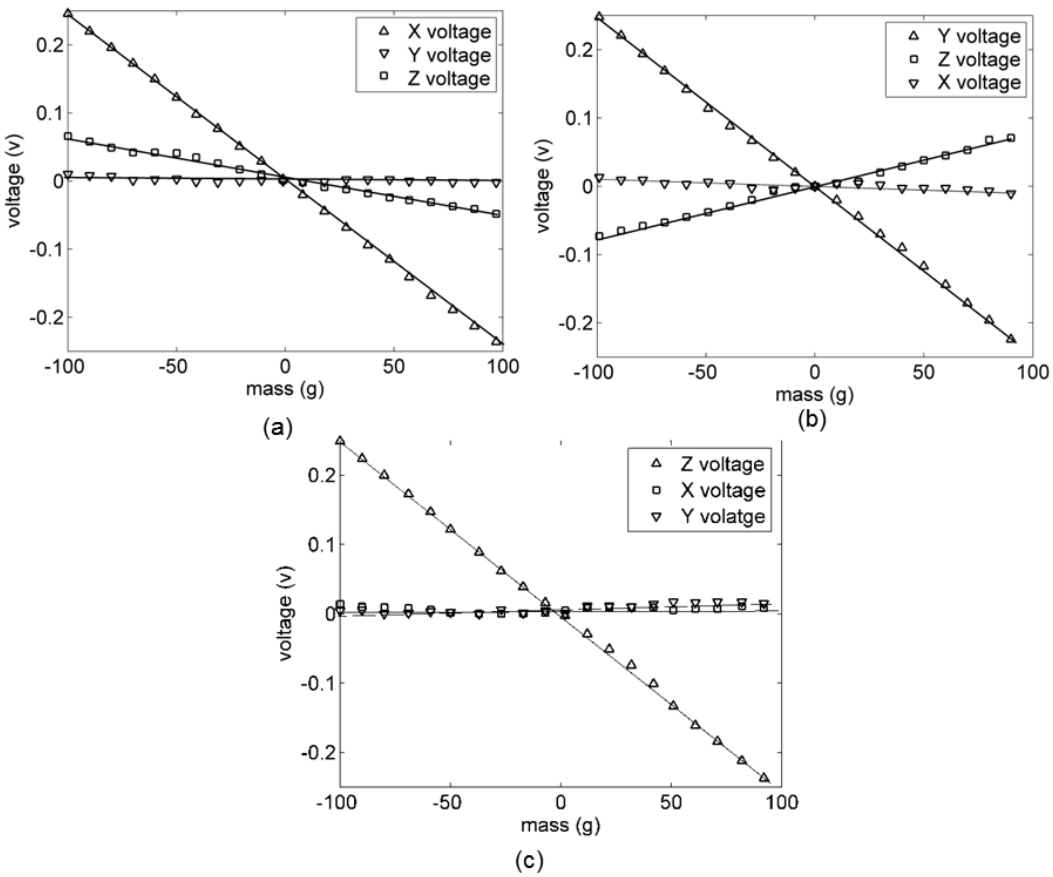

Figure 24. Static calibration of the sensor: (a) X stage, (b) Y stage and (c) X stage

multifunction DAQ NI usb-6009 is interface with the software LabVIEW from national instruments.

To test the load-voltage response of the sensor, each axis was loaded in both directions using laboratory weights with a resolution of 1 gram of force. Fig. 24 shows the voltage signal of each sensor when an incremental load was applied in the X, Y and Z directions. Fig. 24(c) shows the calibration of the Z-axis. From the graph, it can be observed that there is, virtually, no cross-talk in this direction. This is expected as the Z-axis is the closest to the fixed plate and the forces need not be transmitted through the reaming axis. Fig. 23(a) and Fig. 23(b) shows the response of the sensor when the X and the Y direction were respectively loaded. The experimental data show the cross-taking in these directions. Although the cross-talk between the axis is an undesired characteristic, the linear nature of the output voltage suggest the existence of a linear-nonsingular transformation that relate the known voltage of a measurement to is corresponding force vector. The transformation is derived by doing a linear fit to the calibration data as:

$$\begin{bmatrix} V_x \\ V_y \\ V_y \end{bmatrix} = \frac{1}{9.8} \begin{bmatrix} -0.0025 & 0.0084 & 0 \\ 0 & -0.0025 & 0 \\ -0.00061 & 0 & -0.0025 \end{bmatrix} \begin{bmatrix} F_x \\ F_y \\ F_z \end{bmatrix} \quad (13)$$

Where V_i (i = 1, 2, 3) is the voltage in Volts and $F_i$is the force in mN. The diagonal elements of the linear transformation result from the fact that the sensor was designed to have similar stiffness in all of the axis.

4.2.5 Tying a knot

To prove the concept and show the functionality of the sensor, the device was tested by continuously reading the 3D force generated when tying a knot between two threads attached to the end-effector. Even though, only one of the trials is shown, this test was carried several times and the results where reputable throughout all of the trials. Figure 25(a) shows a schematic of

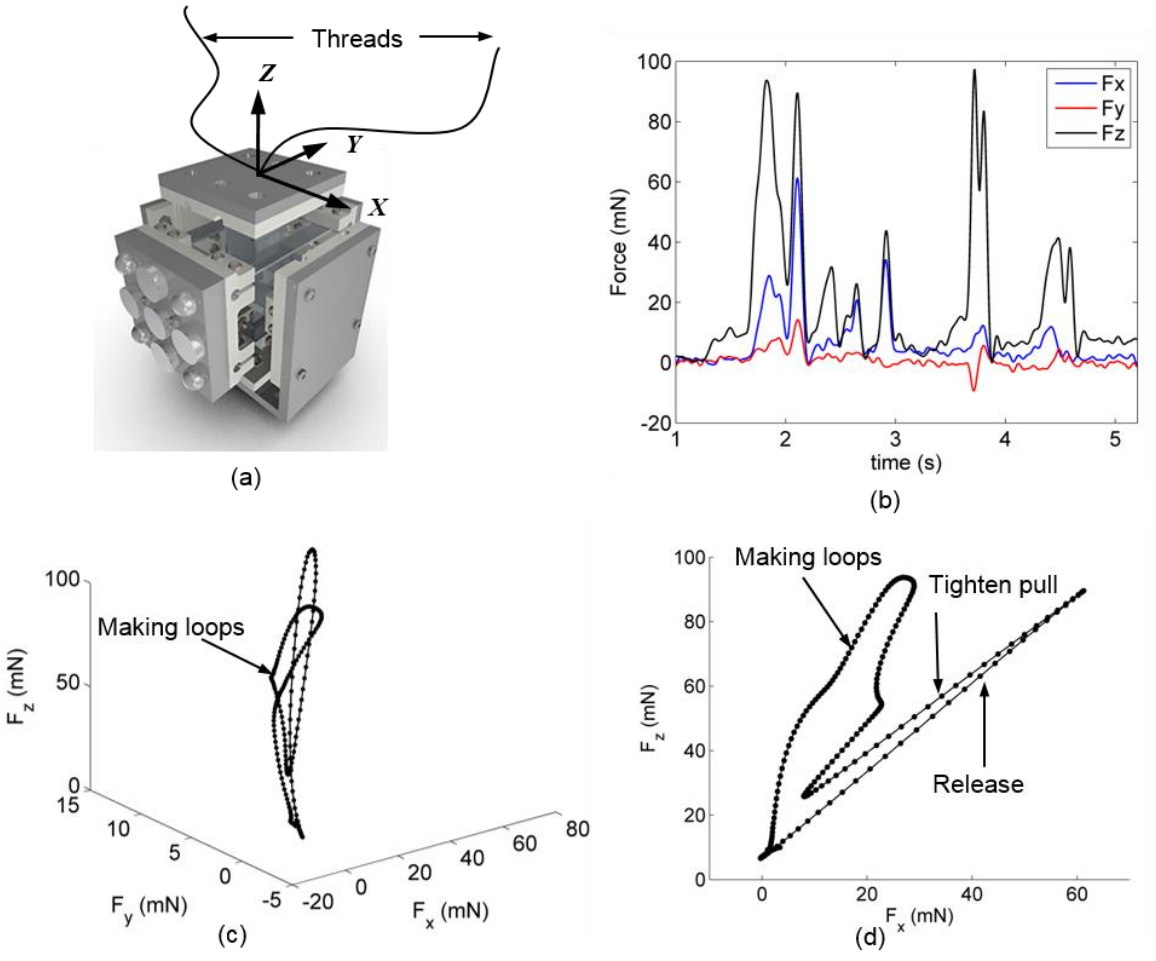

Figure 25 Measurement of the forces when tying a simple knot.

(a) Experiment schematics; (b) sensor output as a function of the time: (c) space and time evolution of the 3D force vector; (d) projection of (d) onto the XZ force plane.

the setup while Fig. 25(b) shows the evolution of each of the forces as a function of time during the tying action. A better insight of the time evolution of forces is obtained by tracking the force vector in the 3D Cartesian space (see Fig 25. (c)). In this form, the time-rate change of the force vector is related to the spacing between the points along the path. This result proves that this low cost system is able to detect forces within the specified ranges and thus, that the design principles presented in this project can be apply to developed cost-effective, potential applications in the areas of precision engineering, micro sensors for medical and automotive industries and portable sensing devices.

CHAPTER 5: FUTURE WORK

To the best knowledge of the author, this thesis work is the first of its kind and it successfully demonstrates functional hybrid-flexure-based devices with extensive information on the design strategies used and their experimental characterization. However, a thorough experimental validation of the interactions at the compound interfaces is still required. To address this issue, a further analysis of the mechanics of deformation and delamination modes and their relation to the manufacturing process is proposed as future work.

The approach of splitting to the manufacturing of hybrid flexural pivots into the manufacture of the mechanism structures and the manufacturing of the leaf sprigs, has the disadvantage of introducing extra assembly steps, contact mechanics, stress concentrators at the interfaces between the host and the inserts and loss of alignment and registration. This problems cannot be avoided and therefore, the mythology in this work is aimed to optimized the mechanics of this elements and facilitate their manufacturing aspects. However, this strategy provides an opportunity to the integration of active components (stamps) within the inserts before assembly and in-situ fabricated strain gauges (See Figs. 27 (b) and 27 (c)). This concept has the potential of producing active joints with load and angular displacement sensing capabilities. This is particularly important in the areas of micro-robotics. Alternative future work topics for this thesis project are:

- Experimental comparison between the hybrid flexures and their conventional, monolithic counterparts
- Redesign of the hybrid flexures to include peg holes as a mechanism of alleviating press fitting stresses and provide post assembly contact enhancement (by insertion of

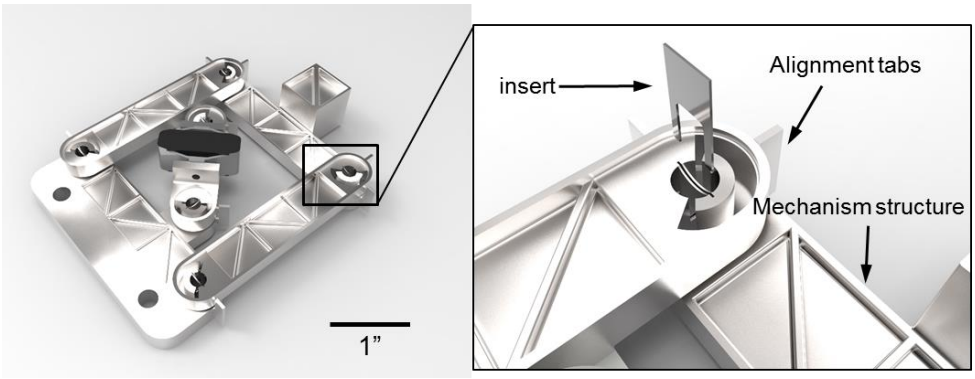

Figure 26. A rendered example of a metal 3d printed 4-bar mechanism with hybrid flexural pivots

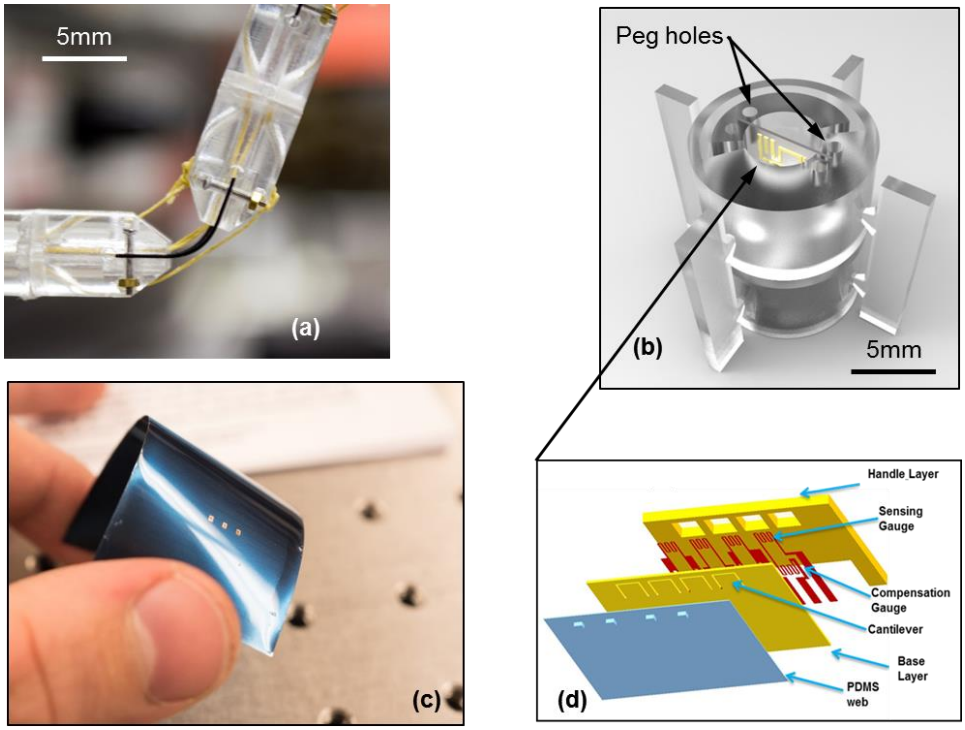

Figure 27. Proposed future work concepts.

(a) A joint for micro-robotic applications with hybrid flexures. (b) render of a hybrid flexural joint with the integration of active composites. (c) Preliminary results of active composite stamps printed on spring steel and (d) active composite stamp Dr. Numair Ahmed PhD Thesis dissertation

pegs).

- Design manufacturing schemes and interlocking geometries to offload the stresses at the interface
- Design of hybrid-flexural pivots with the Integration of metal-based additive manufacturing technologies (Fig.26)
- Miniaturization of the joints for low cost micro-robotics application (Fig, 27 (a)).
- Development of full polymer joints using insert made with Delrin and rapid prototyped structures. This technology has the potential of been used in MRI applications
- Explore low-cost manufacturing approaches to the fabrication of the inserts such as metal sheet shearing, and laser cutting.

CONCLUSIONS

This thesis work presents a novel design methodology, manufacturing aspects and relevant examples of flexure based mechanism mechanisms with hybrid flexural pivots. This manufacturing scheme is of extreme relevance in the context of growing additive manufacturing technologies and has the potential of providing a means of realization of low cost, high performance flexure-based devices for applications in the area of motion engineering, robotics and medical industry.

Some of the technical aspects studied in this work include the use of the pin-joint model as initial design criteria to dimension the flexures given their application requirements. We implemented a simplified-2D finite element model to study the mechanics of the flexure and the interface between the metallic and polymer components. Preliminary structural analysis revealed two main mechanisms of stress concentration, namely, the localized contact stresses and notch tip stresses. Further parametric analysis on this model was used to evaluate the strain energy distribution in the insert and the host material for different penetration lengths using and optimum interfaces between the inserts and the host material. This set of computational experiments resulted in a define relation of the optimal penetration distance with the selection of materials in the joint and the thickness of the flexure. We proposed a strategy based on analyzing the effect of pre-stressing the interface that resulted in a systematic approach to calculate the required amount of interference for a required rotation in order to avoid delamination. Finally, we proposed a fracture mechanics-based failure criteria for flexural pivots in which the underlying idea is to experimentally identify values limiting values of K_I for different set of materials and dimensions of the interface.

To validate the theoretical work in this thesis, we demonstrated examples of two different devices in the areas of motion engineering and medical training. The devices were shown to perform satisfactorily and they represent a repertory of creative design solution applicable to the design of devices with hybrid flexures. Finally, a number of concepts were proposed as future work including the integration of hybrid components with the inserts and implementation of the this this technology in the micro-robotics field.

BIBLIOGRAPHY

[1] L. Howel, Compliant Mechanisms, New York: Wiley, 2001.

[2] N. Lobontiu, Compliant mechanism: design of flexures hinges, CRC press, 2003.

[3] J.Dong, "A novel parallel-kinematics mechanism for integrated, multi-axis nanopositioning Part 2: Dynamics, control and performance analysis.," *Precision Engineering 32 (2008) 20–33,* p. 32 20–33, 2008.

[4] J. Dong, "A novel parallel-kinematics mechanisms for integrated, multi-axis nanopositioning Part 1. Kinematics and design for fabrication," *Precision Engineering 32 (2008) 7–19,* p. 32 7–19, 2008.

[5] M. L. Culpepper and G. Anderson, "Design of a low-cost nano-manipulator which utilizes a monolithic, spatial compliant mechanism.," *Precision engineering,* vol. 28(4), p. 469–482, 2004.

[6] A. Dunning, N. Tolou and J. Herder, "A compact low-stiffness six degrees of freedom compliant precision stage.," *Precision Engineering,* 2012..

[7] A. Shorya and A. H. Slocum, "Topology evolution of high performance xy flexure stages.," *In Proc. ASPE Annual Meeting, Norfolk, VA, Paper,* p. 1802., 2005.

[8] K. Alok and D. W. Rosen, "Building around inserts: methods for fabricating complex devices in stereolithography.," *Rapid Prototyping Journa,* vol. 7(5), p. 253–262, 2001..

[9] M. Constantinos, J. D. Kathryn, W. Jey and A. Munshi, "Fabrication of nonassembly mechanisms and robotic systems using rapid prototyping," *Joural of Mechanical Design,* vol. 123, p. 516, 2001.

[10] L. Hod, C. M. Francis, H. Jimmy and P. Carlo, "3-d printing the history of mechanisms.," *Journal of Mechanical Design, ,* vol. 127, p. 1029, 2005..

[11] T. Laliberte, C. M. Gosselin and G. Cote, "Practical prototyping.," *Robotics & Automation Magazine, IEEE,*, vol. 8(3), p. 43–52, 2001..

[12] C. Yonghua and Z. Chen, "Joint analysis in rapid fabrication of non-assembly mechanism.," *Rapid Prototyping Journal*, vol. 17(6), p. 408–417, 2011..

[13] B. D. Jensen and L. L. Howell, "The modeling of cross-axis flexural pivots," *Mechanism and machine Theory*, vol. 37, pp. 461-476, 2002.

[14] N. Ahmed and P. M. Ferreira, "Close loop control of soft Active composites," *Proceeding of the ASME 2015 International Mechanical Engineering Congress & Exposition*, 2015.